Journal of Energy Storage 81 (2024) 110280

Contents lists available at ScienceDirect

Journal of Energy Storage

journal homepage: www.elsevier.com/locate/est

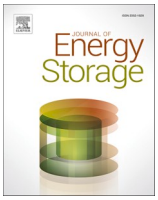

Research Papers

Overcoming the performance limitations of hybrid redox flow batteries with modular operation

Diarmid Roberts [a], Jenny Baker [b], Justin Searle [b], Tom Griffiths [b], Richard Lewis [b], Solomon Brown [a,*]

[a] Department of Chemical and Biological Engineering, The University of Sheffield, Sheffield S10 2TN, United Kingdom
[b] SPECIFIC, College of Engineering, Swansea University Bay Campus, Swansea SA1 8EN, United Kingdom

ARTICLE INFO

Keywords:
Hybrid redox flow battery
Zinc bromine
Modular
Maintenance scheduling
Firm PV
Self-sufficiency

ABSTRACT

To help solve the energy trilemma, energy storage technologies must demonstrate low cost and high efficiency to avoid inflating the cost of renewable power. Hybrid redox-flow batteries are a promising multi-hour storage technology, as they use low cost chemicals in an easily recyclable format. However, they suffer from low efficiency at low power output, and require periodic maintenance downtime to remove metal from the anode. Here, we show that a modular system can overcome these challenges with appropriate control. A novel optimisation model for modular operation with periodic maintenance is parametrised from a commercial zinc-bromine hybrid RFB. Independent module control was predicted to improve operational efficiency, with six modules achieving 73 % compared to the peak efficiency of 80 %. A non-obvious schedule for maintenance was determined algebraically, where energy is transferred from a module due maintenance to one that is fresh. It is found that staggering the strip cycles across several days and performing them when PV and load are roughly in balance in the morning is the optimal timing. The findings are significant as they show that maintenance does not preclude hybrid RFB from firm power provision, and that high efficiency is possible during operation through modular control.

1. Introduction

In 2019 buildings accounted for over 35 % of total energy demand in the UK [1]. This is split between appliances and heating demand, with 65 % of households using gas to heat their homes [2]. The Sustainable Product Engineering Centre for Innovative Functional Innovative Coatings (SPECIFIC) has produced a number of demonstrator buildings to showcase technologies that enable buildings to operate without the need for fossil fuels and by providing enough energy to meet their own consumption needs [3]. Removing the need for fossil fuels is primarily achieved through electrification although some technologies, such as thermal/PV hybrids [4] and transpired solar collectors [5], produce direct heat for hot water demand and pre heating heat pump intakes.

This study focuses on the Active Classroom, a demonstrator building built by SPECIFIC at the Swansea University Bay Campus, South Wales, where electricity demand is primarily met from rooftop PV (16.2 kWp) [6,7]. Demonstrators are an essential part of the transition to a more sustainable energy system, de-risking the technologies for investors and highlighting practical advantages and obstacles that need to be overcome before mass implementation. In May 2020 12 × 10 kWh Zn—Br redox flow batteries (RFBs) were installed in order to store excess PV and also to provide support to the grid at times of higher demand.

RFBs differ from conventional batteries, such as lead acid (LAB) or lithium ion batteries (LIB), in that instead of the energy being stored in the active material within the electrode the energy is stored within the liquid electrolyte in the form of dissolved active materials, which undergo oxidation and reduction.

RFBs are available in many different chemistries such as Fe/Cr [8], polysulfide halide [9], Pb/PbO [10], Zn/Br [11] and vanadium based [12]. Lead based RFBs that use similar chemistry to standard lead acid batteries are being developed as a low cost technology particularly for use in rural mini grids where the known chemistry and ability to recycle [13] is of particular advantage, although additives are sometimes needed to improve cycle life [10]. There are a number of key advantages of RFBs noted by Ravikuma et al. [14]; good reversibility of electrolyte reactions, tolerance to higher ambient temperatures (e.g. up to 50 °C for the Zn/Br system [15]), reducing infrastructure costs, low risk of fire,

* Corresponding author.
E-mail address: s.f.brown@sheffield.ac.uk (S. Brown).

https://doi.org/10.1016/j.est.2023.110280
Received 3 April 2023; Received in revised form 8 December 2023; Accepted 22 December 2023
Available online 13 January 2024

Nomenclature

Indices

S	Set of *s* modules in the ensemble
T	Set of *t* hourly time-steps

Decision variables (continuous, positive)

$I^{C}_{s,t}$	Hybrid RFB module charge current at time *t* (A)
$I^{D}_{s,t}$	Hybrid RFB module discharge current at time (A)

Indicator variables (binary)

$\delta^{C}_{s,t}$	Takes value of 1 if hybrid RFB module charging at time *t*, otherwise 0
$\delta^{D}_{s,t}$	Takes value of 1 if hybrid RFB module discharging at time *t*, otherwise 0
$\delta^{Imp.}_{t}$	Takes value of 1 if there is a power deficit at the site, 0 otherwise
$\delta^{Exp.}_{t}$	Takes value of 1 if there is a power surplus at the site, 0 otherwise

Exogenous variables (continuous, positive)

P^{load}_{t}	Electrical load at site (excluding hybrid RFB) at time *t* (kW)
P^{PV}_{t}	Output of photovoltaics at site at time *t* (kW)

Dependent variables

$P^{RFB}_{s,t}$	Dependent variable: power consumption of hybrid RFB module at time *t* (kW)
nl_t	Dependent variable: net load at site at time *t* (kW)
C_s	Capacity of hybrid RFB module *s* (Ah)

Parameters

Δ_s	Maximum permitted interval between strip cycles (h)
$I^{C.Max}_{s}$	Maximum charge current of hybrid RFB module *(A)*
$I^{D.Max}_{s}$	Maximum discharge current of hybrid RFB module *(A)*
I^{Loss}_{s}	Parasitic loss of current from hybrid RFB module while active (A)
l_s	Length of strip cycle (h) for hybrid RFB module
P^{pump}_{s}	Power consumption of hybrid RFB module pump when active (W)
R_s	Internal resistance of hybrid RFB module stack (Ω)
τ	Model time-step (h)
V^{k}_{s}	Kinetic overpotential of hybrid RFB module stack (V)
V^{stack}_{s}	Representative voltage of hybrid RFB module (V)

high cycle life and deep discharge operation. The simple design lends RFB to ease of recycling at end of life. This is critical to avoid excessive materials resource depletion, which is a risk if the focus is only on reducing emissions of greenhouse gases [16]. Vanadium based RFB (VRFB) are the most commercialised with individual systems of 1 MWh connected to the grid in 2017 [17] and larger installations of 5 MWh planned to support the grid in Oxford, UK as part of a lithium/VRFB hybrid system [18]. However, when batteries were being sourced for the Active Classroom in 2019 VRFBs were only commercially available in the UK within shipping containers, which was too large for the building. Instead, the system installed was based on the ZBM2 module manufactured by Redflow, a small (3 kW / 10 kWh) modular Zn/Br system that enables the user to connect multiple batteries together to create an installation of the size required by the customer [15].

Zinc-bromine RFB [11] are often termed 'hybrid' RFB as the zinc is deposited on to the electrode during charging and then dissolves on discharge (Eq. (2)).

$$Zn^{2+}(aq) + 2Br^{-}(aq) \rightarrow (charge)\ Zn(s) + Br_2(aq)$$

$$Zn(s) + Br_2(aq) \rightarrow (discharge)\ Zn^{2+}(aq) + 2Br^{-}(aq)$$

A potential problem with hybrid RFB is that uneven deposition may occur and become progressively worse across multiple charge-discharge cycles. If deposition is thicker in a certain area, then during discharge an isolated patch may be left as the rest of the electrode becomes bare, and the stack voltage drops to the cut-off. One of the conditions on the longevity of these Zn/Br hybrid RFB is the periodic performance of a 'stripping cycle', where the battery must be discharged to an apparent SOC of 0, then discharged for an additional period in case any localised deposits remain [19]. This reduces the availability of a module, and may impact on usability. The use of metal plating also limits the extent to which power and energy rating re decoupled, when compared to an all solution RFB.

Another potential limitation of the system is that the high coulombic efficiency highlighted by Ravikuma [14] does not always result in high efficiency during practical operation due to the requirement to keep the electrolyte agitated and pump electrolyte around the system. Also, as in all RFBs, parasitic shunt currents within the electrolyte manifold

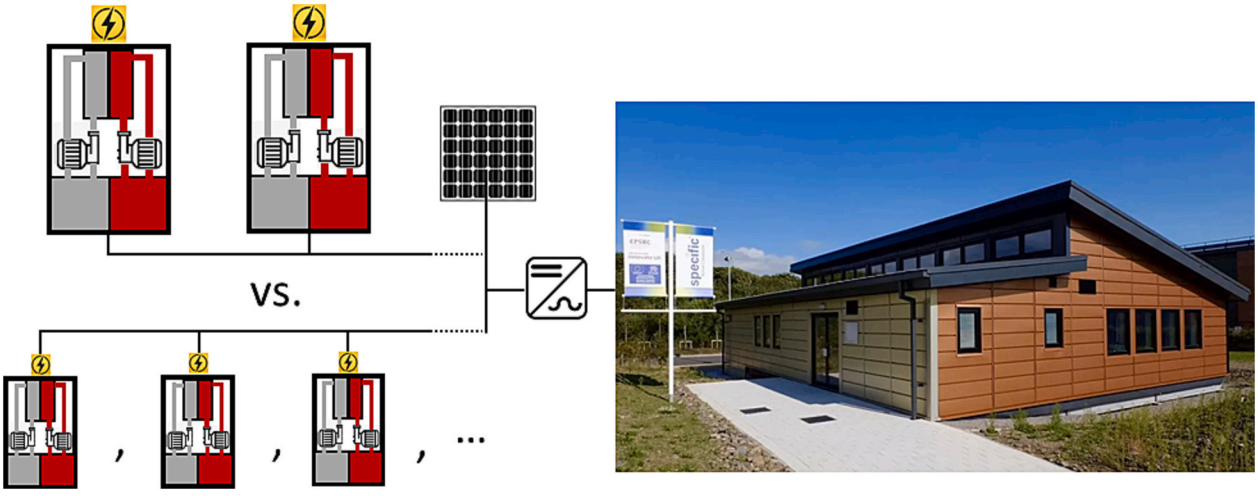

Fig. 1. Schematic of the Active Classroom site, where zinc-bromine hybrid RFB are installed alongside PV on a DC bus to power a demonstration educational facility [7]. The two possible RFB configurations represent different degrees of modularity, the benefits of which are investigated in this article.

contribute to self-discharge. These losses can be approximated as constant, hence at low power utilisation the efficiency of the RFB becomes poor. Where the RFB is connected to the grid within a trading paradigm this is not such a problem, as the owner can choose when to operate, trading off efficiency and price signals [20]. However, where the RFB must follow a load or PV output profile, as in a micro-grid application, this is not an option. In fact, the gap between advertised efficiency and that achievable in the field was mentioned in a recent industry discussion on factors holding back the commercial rollout of RFB systems [21].

This work is based on the hypothesis that a modular system with individual module control will be better able to overcome these issues than a single large system treated as a homogenous bank. We formulate, for the first time, an algebraic optimisation model that is able to quantify the impact of the maintenance and efficiency limitations mentioned above, and optimise around them for any number of modules.

Using data from the Active Classroom demonstrator, we investigate these impacts in the context of a micro-grid powered by photovoltaics. The case study is schematised in Fig. 1.

2. Methods

2.1. Optimisation model

The operation of the hybrid RFB battery array is optimised using a mixed integer-quadratic programming (MIQP) method based on the approach described by Roberts et al. [20]. In order to include the consideration of the modularity of the system, this model is expanded to consider the scheduling of the individual modules rather than the system as a whole.

This model is posed in terms of current rather than current density, as the performance data given in the following section are reported in these terms. For S RFB modules, the net load at the site in time-step t is defined by:

$$nl_t = P_t^{Load} - P_t^{PV} + \sum_{s \in S} P_{s,t}^{RFB} \tag{1}$$

where P_t^{load} and P_t^{PV} are the exogenous variables site load and PV output (kW), and $P_{s,t}^{RFB}$, the power consumed by RFB module s at time t (kW) is defined by:

$$P_{s,t}^{RFB} = \left(I_{s,t}^{C}\left(V_s^{stack} + V_s^{k}\right) - I_{s,t}^{D}\left(V_s^{stack} - V_s^{k}\right) + R_s\left(\left(I_{s,t}^{C}\right)^2 + \left(I_{s,t}^{D}\right)^2\right) + P_s^{pump}\left(\delta_{s,t}^{C} + \delta_{s,t}^{D}\right) \right) \Big/ 1000 \tag{2}$$

where $I_{s,t}^{C}$ and $I_{s,t}^{D}$ are continuous positive decision variables for charge and discharge current, $\delta_{s,t}^{C}$ and $\delta_{s,t}^{D}$ are binary indicator variables for charge/discharge state, P_s^{pump} is the power consumed by the pump while running, V_s^{stack} is the representative module stack voltage, V_s^{k} is a scalar approximation of the kinetic over-potential and R_s is the stack resistance.

As a surplus of power ($nl_t < 0$) is only useful for self-sufficiency if stored in the RFB, it is necessary to make a binary distinction between surplus and deficit. Continuous auxiliary variables $P_t^{Imp.}$ and $P_t^{Exp.}$ are defined representing the import and export power at time-step t. These are then constrained to take the value of the net load when appropriate by:

$$nl_t = P_t^{Imp.} - P_t^{Exp.} \tag{3}$$

and:

$$P_t^{Exp.} - M\delta_t^{Exp.} \leq 0 \tag{4}$$

$$P_t^{Imp.} - M\delta_t^{Imp.} \leq 0 \tag{5}$$

$$\delta_t^{Imp.} + \delta_t^{Exp.} \leq 1 \tag{6}$$

where M is a 'big M' type number [22], and $\delta_t^{Imp.}$ and $\delta_t^{Exp.}$ are binary indicator variables. The idling of the RFB module is approximated by assuming that when no current flows through the terminals, there is no parasitic current (pump and fan off, no shunt currents as bromine phase settles out of stack). To ensure non-zero current results in the 'active' condition during charging module s is constrained by:

$$I_{s,t}^{C} - I_s^{MaxC}\delta_{s,t}^{C} \leq 0 \tag{7}$$

And the converse condition by:

$$I_{s,t}^{C} - \mu\delta_{s,t}^{C} \geq 0 \tag{8}$$

where $\delta_{s,t}^{C}$ is a binary indicator variable, and μ a small but non-zero number [23]. The same constraints are applied to the discharge variables $I_{s,t}^{D}$ and $\delta_{s,t}^{D}$. Charge/discharge exclusivity is enforced by:

$$\delta_{s,t}^{C} + \delta_{s,t}^{D} \leq 1 \tag{9}$$

The state of charge of RFB module s at time t is defined by:

$$SOC_{s,t} = SOC_{s,t-1} + \left(I_{s,t}^{C} - I_{s,t}^{D} - \left(\delta_{s,t}^{C} + \delta_{s,t}^{D}\right)I_s^{Loss}\right)\frac{\tau}{C_s}$$

where I_s^{Loss} is the fixed coulombic loss (A) while active, τ the model time-step (h) and C_s the coulombic capacity (Ah).

The objective of the optimisation, to maximise self-sufficiency, is defined by:

$$minimise\left(\left(\tau\sum_{1}^{w/\tau} P_t^{Imp.} - a\sum_{s} C_s V_s^{stack} SOC_{s,w/\tau}\right)\right) \tag{11}$$

where the second term is an incentive term (kWh) that encourages the storage of any surplus PV beyond that required to satisfy the load in the current optimisation window. a is an arbitrarily small coefficient (1×10^{-5} was used in this case study).

The self-sufficiency ratio (SSR) may subsequently be calculated for any period by:

$$SSR = 1 - \frac{\sum_t P_t^{Imp.}}{\sum_t P_t^{Load}} \tag{12}$$

following the definition in [24].

The additional constraints regarding the bounds on SOC and current are analogous to those found in [20] excepting the multiple module index S, and the current variables being specified in A rather than A m^{-2}.

2.2. Maintenance constraints

In the ZBM2 manual, it is stated that a strip cycle would optimally be performed after every full discharge, but at a minimum, after every 72 h of zinc electrolyte (anolyte) pump operation. In this work, the latter condition is simplified so that maintenance must be performed every 72

h of clock time. This is a conservative approximation, as the RFB would not necessarily be active 24 h a day.

For each module s, a maximum period of Δ_s is allowed between maintenance cycles, which consist of discharging the battery to zero SOC then spending l_s hours at SOC = 0. During the strip cycle the pump must keep running to supply electrolyte to complete the redox reaction. In this model, the associated power consumption is neglected, as it is minor, but would be an important practical consideration if a single module was being used off-grid.

In the optimisation period W, there are as many as W - Δ_s periods in which a maintenance cycle must occur (see note on exception where W > Δ_s in 2.3). The set $\boldsymbol{M}_s$ is first defined, containing the earliest time step in each of these periods. As the operation is being optimised on a rolling window, the modules do not necessarily start with 0 h on the maintenance timer, hence for each module it is necessary to define the additional set H_s at the start of the window, comprising the time-periods that satisfy:

$$0 < t < \frac{\Delta_s - TSLS_s}{\tau} \tag{13}$$

where $TSLS_s$ is the time since the last strip cycle of module s.

A binary decision variable $\delta_{s,t}^{strip}$ representing strip cycle initiation is then defined for each module s and time-step t. The general maintenance periodicity of module s is then enforced by:

$$\sum_{t}^{t+\Delta_s/\tau} \delta_{s,t}^{strip} = 1 \forall t \in \boldsymbol{M}_s \tag{14}$$

And the historical requirement by:

$$\sum_{t} \delta_{s,t}^{strip} = 1 \forall t\, H_s \tag{15}$$

The requirement that module s be taken to 0 SOC before initiating the strip cycle, and then kept there for the following l hours is enforced by:

$$\sum_{t}^{t+l/\tau} SOC_{s,t} \leq \left(1 - \delta_{s,t}^{strip}\right) . \frac{l}{\tau} . SOC_s^{max} \forall t \in \boldsymbol{M}_s \tag{16}$$

With the last two terms providing the tightest possible 'big M' value outside of maintenance periods. It is assumed that the maintenance period set for the system is short enough that the available capacity of the module does not change by a meaningful amount due to build-up of less accessible zinc deposits.

2.3. Progression of optimisation window

In this work, the schedule optimisation is performed one day at a time, in order to avoid applying the perfect forecasting assumption to unrealistically long periods. This presents a challenge to the strip cycle optimisation, as this is constrained to be once every 72 h. A heuristic is hence applied, whereby the constraints in Section 2.2 are only applied if a strip cycle is obligatory, that is if $TSLS_s + W > \Delta_s$.

Optimising 24 h at a time may lead to an infeasibility error in the 4th window, where the strip cycle is due in the first hour, but the SOC is not 0 (violating eq. 16). To avoid this a rolling window is used, where the optimisation is done on the next 28 h of data, but only the first 24 h of the schedule is implemented.

The full code and the data required to reproduce the case study are hosted in a GitHub repository [25].

2.4. Computation

The 28 h (56 period) optimisation problems were posed using PYOMO [26] and solved with Gurobi [27], on a system with up to 128 Gb of RAM and 2× Intel Xeon CPU E-2620 v4, 2.1GHz (8 cores and 16 threads). The termination condition for the branch and bound process was set at whichever was reached first from a time limit of 600 s and a gap between best integer-feasible solution found and best LP relaxed bound of 0.01 %.

Table 1
Performance parameters for Zn|Br modules.

Parameter	Description	Value	Units
R_s	Internal resistance of stack	0.1	Ω
V_s^{stack}	Representative stack voltage	52	V
V_s^a	Kinetic overpotential	0	V
P_s^{pump}	Pump power while active	60	W
Δ_s	Maximum strip cycle interval[a]	72	h
l_s	Strip cycle downtime @ SOC = 0	2	h
$I_s^{C.Max}$	Max current charge	50	A
$I_s^{D.Max}$	Max current discharge	90	A
I_s^{Loss}	Parasitic loss	1.3	A
C_s	Capacity	220	Ah

[a] This is a simplification of the manual description, as discussed in Section 2.2.

2.5. Time series data

In order to demonstrate the modular operation over a range of climatic conditions, site load and PV output data were taken from Q4 2020 for the Active Classroom. This data may be found alongside the code in a GitHub repository [25].

2.6. Battery specification

In the present work, the hybrid RFB is based upon the ZBM2 Zn/Br product from RedFlow [15]. Table 1 presents performance parameters for a single module used in this study.

The parameters were taken from the manual [28], apart from the following: V_s^a is set to 0, as all of the voltage drop from the 100 % SOC float voltage of 54 V to the initial working voltage of 53 V seen in the product datasheet at C20 may be accounted for by ohmic losses (11 A X 0.1 Ω = 1.1 V) [15]. The representative open circuit voltage of the stack (V_s^{stack}) was taken from the midway point of the C20 discharge curve, adding back the estimated 1 V due to ohmic losses. I_s^{Loss}, the parasitic loss was inferred from the statement in the manual that the ZBM2 may be drained from 100 % SOC in 7 days using just the pumps and the fan (220 Ah/168 h =1.3 A). It is assumed that the parasitic losses during charging are the same as those inferred for discharge. This assumption is reasonable: in a study from Sandia National Laboratories of an earlier embodiment of the ZBM2 module, the coulombic efficiency was the same for 15 A charge/30 A discharge and 30 A charge/15 A discharge cycles [29].

Although the Active Classroom has a battery of 12 ZBM2 modules, this system is oversized relative to the site load and PV output. This is because it was specified for additional grid support activities and to enable battery research to be undertaken whilst still enabling the classroom to operate. In order to make the case study more realistic, a battery of just 6 ZBM2 modules was simulated, which would be able to accept the maximum observed PV output of 13.5 kW [25] from the 16.2 kWp array [7] at the maximum charging power per module (50 A X 52 V = 2.6 kW) [25].

Four modularity cases are simulated in this work:

- 1 block: all modules are given the same instructions.
- 2 blocks of 3 modules: independent control of blocks, synchronised control within each block.
- 3 blocks of 2 modules: control as above.
- 6 blocks: each module controlled independently.

In the simulation of strip cycle maintenance, all modules are assumed to be stripped prior to the study, so the *TSLS* counter is initially set to 0.

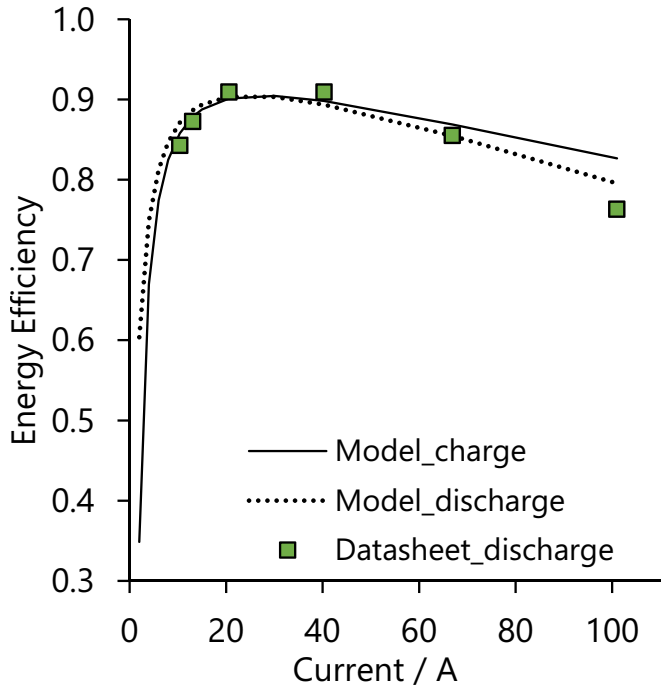

Fig. 2. Modelled efficiency of single RFB module vs. RedFlow datasheet. The datasheet only includes discharge efficiency data.

3. Results

In this section we explore the benefits of individual module control for self-sufficiency at the Active Classroom site. To do this, the simulation is performed over sixteen weeks of data starting from the 1st September 2020, which covers a range of climatic conditions from surplus PV to PV deficit. In the following sections, the model for RFB efficiency is first compared to reported data. Then the benefit to efficiency of modular operation is tested. Lastly, the ability of a modular system to avoid downtime for strip cycle maintenance is tested.

3.1. Comparison of model data to reported performance

Although the fixed parasitic loss is the same in the model during both charging and discharging, the modelled efficiencies deviate at low current. This is because the RFB spends longer charging than discharging (E.g. for a 2 A cycle, internal charge current is 2 A - 1.3 A, whereas internal discharge current is 2 A + 1.3 A), hence the total parasitic power consumption is greater. The deviation at high current has a similar explanation relating to ohmic overpotential. Overall, the MIQP representation of efficiency gives good agreement with the reported figures.

3.2. The benefit of modularity under micro-grid self-sufficiency objective

In the self-sufficiency case, closely matching the PV surplus during charging, and the site load during discharging becomes crucial, as any charging from the grid is discouraged, or in many situations may not be possible. The Active Classroom case study is potentially challenging for a flow battery as the site load is often very low, which may lead to poor storage efficiency as shown in Fig. 2.

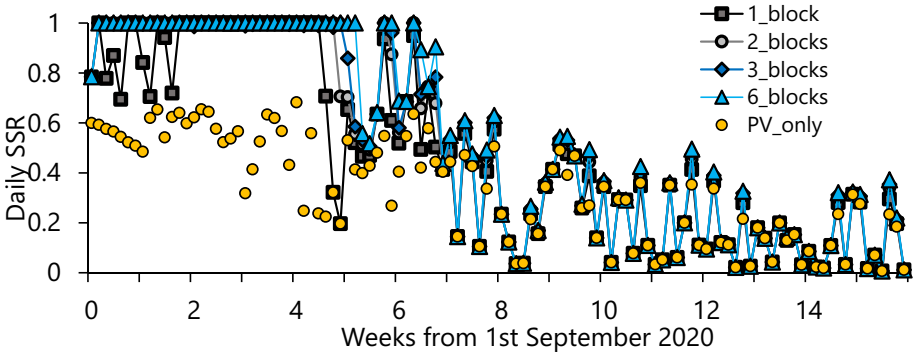

Fig. 3. The modelled daily self-sufficiency ratio (SSR) achieved at the Active Classroom site by a six module RFB operated at different levels of modularity. The SSR achieved with just the PV array (no RFB) is also shown.

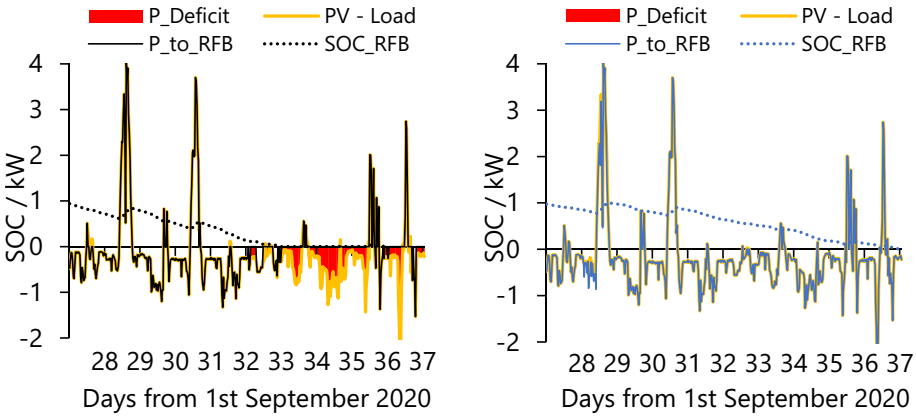

Fig. 4. Snapshots of simulated optimised operation of RFB systems at the Active Classroom in a period where PV output net of load goes from surplus to deficit. Left: RFB modules synchronised to form single block. Right: all six RFB modules operated independently.

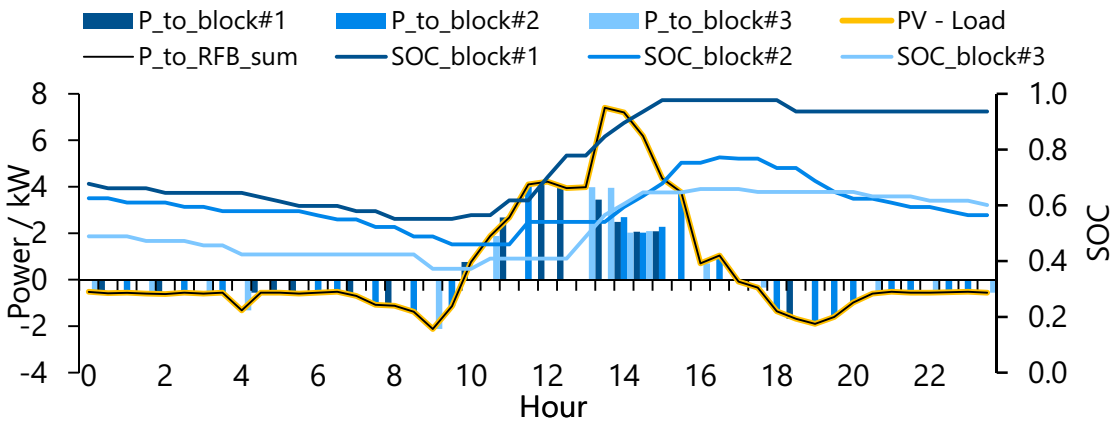

Fig. 5. Optimal schedule for 3rd day of 5th week in studied period, showing how individual blocks in the ensemble are dispatched to avoid low current operation.

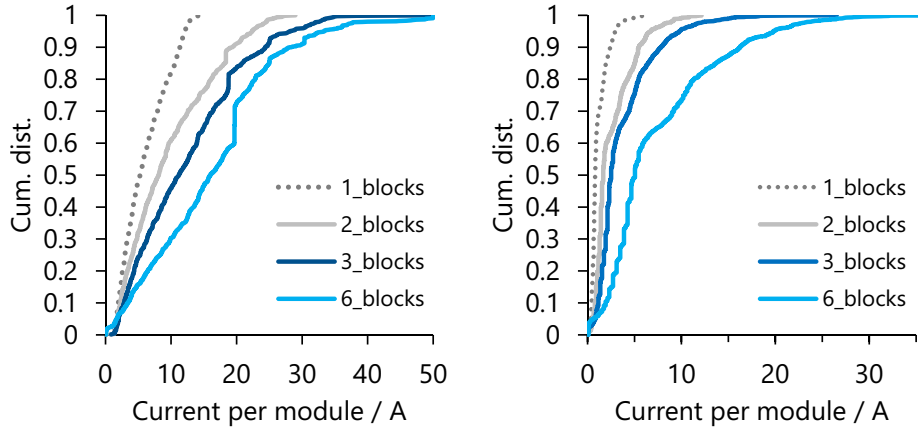

Fig. 6. Cumulative distribution of current per module while active under the 4 modularity scenarios. Left: charge. Right: discharge. Note: in the discharge plot, the 6 block system data includes one period of discharge at 90 A which has been truncated.

To estimate the benefit of modularity four permutations were modelled: 1 block with all 6 modules synchronised, 2 blocks of 3 synchronised modules, 3 blocks of 2 synchronised modules and lastly, 6 individual modules. The operation of each system was optimised 24 h at a time for 16 weeks from September 1st 2020. The daily self-sufficiency ratio achieved at the Active Classroom assuming perfect forecasting is shown in Fig. 3.

Fig. 3 shows that a higher self-sufficiency is achieved as the system is split into greater numbers of independently controllable modules. The increase varies according to the degree of PV surplus; in early September all permutations except 1 block achieve SSR close to 1 on most days. In the later weeks (8–16), there are many days where there is no PV surplus, hence the operation of the RFB has no effect on the SSR. The greatest difference in SSR due degree of modularity is found in the fifth week. This period is shown in greater resolution in Fig. 4.

The period shown in Fig. 4 is ten days of overall PV deficit following a period of surplus in which the RFB is fully charged. The RFB ensemble operated as a single block reaches a SOC of 0 on the 6th day, after which the site would need to import power or suffer outages. The RFB ensemble operated as 6 independent modules is able to continue supporting the site load without deficits for a further 4 days.

The extended discharge of the modular system is due to improved efficiency, which may be explained by reference to Figs. 5 and 6.

Fig. 5 shows how the RFB system split into 3 independently controllable blocks operates during a single day. (Note: the 3 module system is chosen as an example for ease of presentation). Before the Sun comes up, the RFB must cover a very low load relative to its maximum power output. To do this as efficiently as possible, only one module is

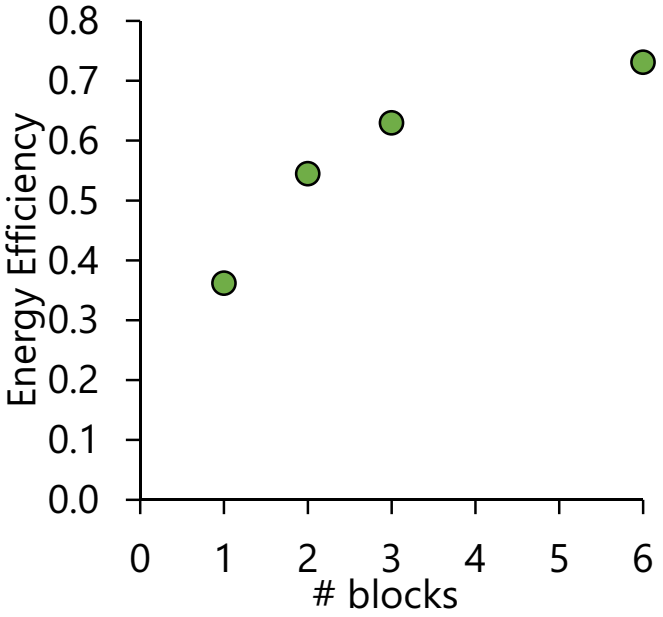

Fig. 7. Modelled operational efficiency of the RFB system across the 16 weeks at the Active Classroom site under different modularity cases.

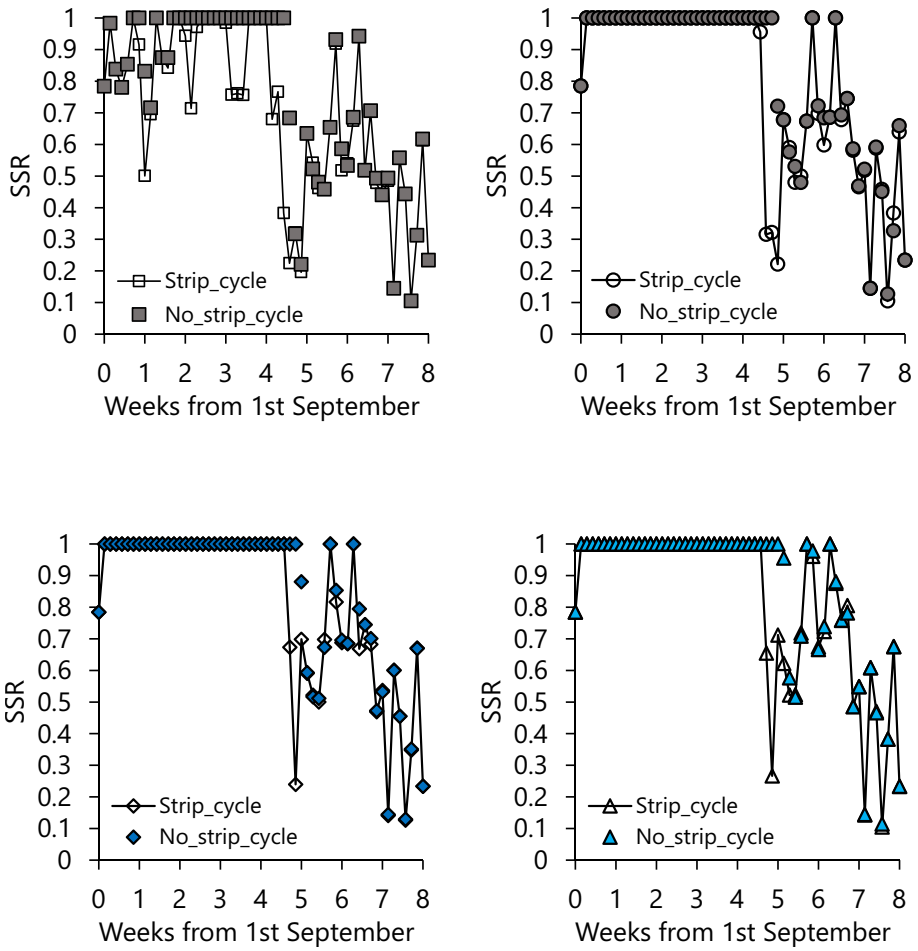

Fig. 8. Impact on self-sufficiency ratio at the Active Classroom site of enforcing strip cycle maintenance constraint on RFB operation. The different modularity cases are shown, from left to right and top to bottom: 1 block, 2 blocks, 3 blocks, 6 blocks.

activated in each period in order to minimise the parasitic losses. During charging from PV, single modules are activated when the surplus is lower, with additional modules brought online at higher surplus to avoid charging at a power rating above the peak efficiency point in Fig. 2.

Fig. 6 shows the distribution of module current (excluding idle periods) across the full 16-week period for the various modularity permutations. For charging, as the number of sub-blocks increases, the distribution is pushed towards higher current densities. From the systems of 2 blocks and above a step appears, where the solver has sufficient freedom to aim for the efficiency plateau shown for charging in Fig. 2. As the block number is increased, this step gets closer to the peak efficiency point of around 25 A shown in Fig. 2. The drop off in efficiency above this peak is less steep than below it, hence the increasing number of charge events at >25 A with block number is less important than the reduction in those at <10 A.

The high asymmetry of charge and discharge current distributions is a feature of this particular case study that may not apply in all cases. However, some asymmetry is intrinsic to firm PV provision as the hours of PV surplus are <50 %.

The variation in operational efficiency was subsequently calculated for each permutation across the 16-week period, as the sum of power output from the RFB divided by the sum of power input. The results are shown in Fig. 7.

Fig. 7 shows that there is a dramatic improvement to the modelled operational efficiency of the RFB system when the RFB is split into independently controlled sub blocks. In this case study, an improvement is seen all the way up to 6 blocks, where each ZBM2 module is controlled independently. However, the efficiency gain is sub-linear with respect to block number.

3.2.1. *The benefit of modularity in avoiding system maintenance downtime*

In Section 3.2, it was assumed that the RFB requires no maintenance. In reality, each module is required to be discharged after 72 h of activity then subjected to a 2 h strip cycle to remove any remaining zinc deposits from the anode.[1] This requirement has the potential to interfere with the provision of firm power, as the module will not be able to charge or discharge during this time. In this section, the impact of maintenance on SSR at the Active Classroom is modelled under the different modularity cases.

In the first analysis, the optimisation window is still performed on a rolling window with the first 24 h of the 28 h optimisation window implemented. As this period is less than the 72 h maintenance period, the constraint is only enforced on the day when maintenance becomes unavoidable. This is an overly constrained scenario, but serves as a worst case. The RFB modules are all initiated with 0 h on the maintenance timer.

The SSR achieved under the different modularity cases is shown in Fig. 8, with and without the maintenance constraint. For clarity the later 8 weeks are not shown – as described previously the RFB would be mostly empty in this period anyway so maintenance would have little impact.

[1] Note, the model formulation is simplified so that the maintenance is required every 72 h of calendar time rather than active time. The model is hence conservative with respect to maintenance requirements.

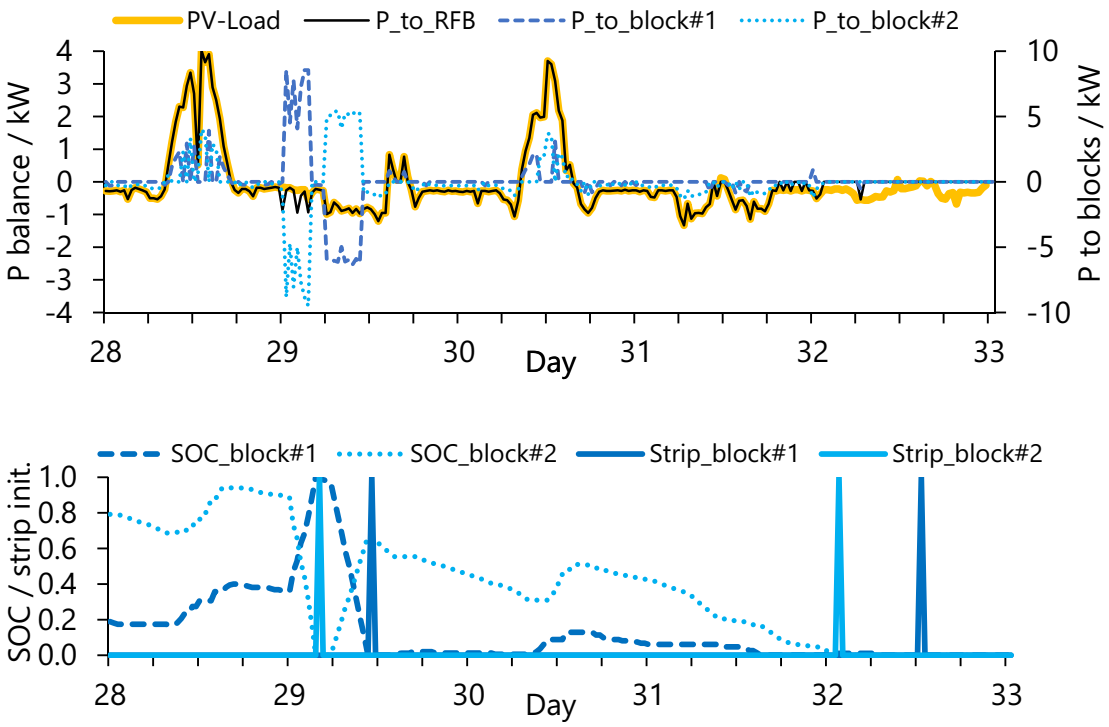

Fig. 9. Snapshot of optimal simulated operation of the 2 block RFB configuration during a period of overall PV deficit. Top: power flows, Bottom: state of charge and strip cycle initialisation timing for each RFB block.

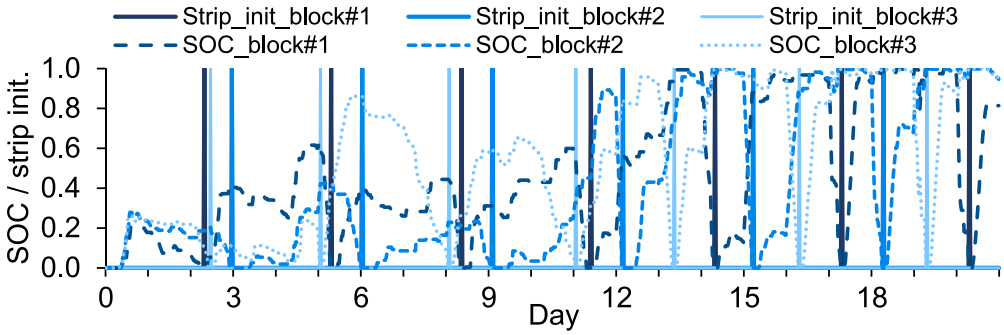

Fig. 10. Plot of SOC and strip cycle initiation timing for the 3 block system in the first three weeks of the studied period.

Fig. 8 shows that the impact of the strip cycle requirement is lessened when the RFB is split into multiple modules. In the first 4 weeks, where there is an overall surplus of PV, it is only necessary to split the RFB into 2 blocks to avoid having any loss of SSR due to the strip cycle constraint. This is because the SOC in one of the blocks will be high enough to support the load while the other is discharged.

For the multi-block scenarios, the strip cycle requirement is seen to compromise the SSR starting in the 5th week. This occurs on day 3 in the 2 block case, and day 5 in both the 3 block and 6 block cases.

Fig. 9 illustrates an important benefit of modular control – the ability to transfer power between modules when one is required to discharge for a strip cycle. On the 30th day, block #1 then block #2 both discharge to 0 SOC. In each case however, the energy in the block is greater than the integral load hence the optimal strategy is to transfer it to the other block. In the first transfer, the energy from block #1 is greater than can be consumed by load or stored in block #2 and a small amount must be exported. In the second transfer, no export is required. This manoeuvre is obviously not an option for a single block system, hence the significant impact of the strip cycle requirement on SSR in Fig. 8.

Although the 2 block system allows the average SOC to be maintained above 0 throughout day 30, there is an efficiency penalty to transferring the power between blocks. Increasing the number of blocks from 2 to 3 further increases the performance of the system under the strip cycle constraint. There are three reasons for this. Firstly, because each block has a smaller capacity, a greater proportion of the energy that must be discharged prior to the strip cycle may be used directly to supply the site load, meaning lower losses. Secondly, when a block discharges there is the option of charging both the remaining blocks, as shown in Fig. 10.

As this is a less constrained situation than in the 2 block case, the solver is able to move the current in each block closer to the optimum shown in Fig. 2. Third, the flexibility offered by three blocks translates to a benefit in strip cycle timing. As seen in Fig. 10, the first strip cycle on each block is performed on day 3. As the simulation progresses, the strip cycle on block #2 gets pushed back by 2 h each period (remembering that the constraint is one strip cycle per 72 h, and 2 h per strip cycle). The motivation for this is that pushing the strip cycle back allows the block to be discharged over a longer period so more of the stored energy can serve the site load directly. Concurrently, the strip cycle initiation on block #3 is moved progressively forward in order to be further from that of block #1.

By the end of the first three weeks the strip cycle timing settles into

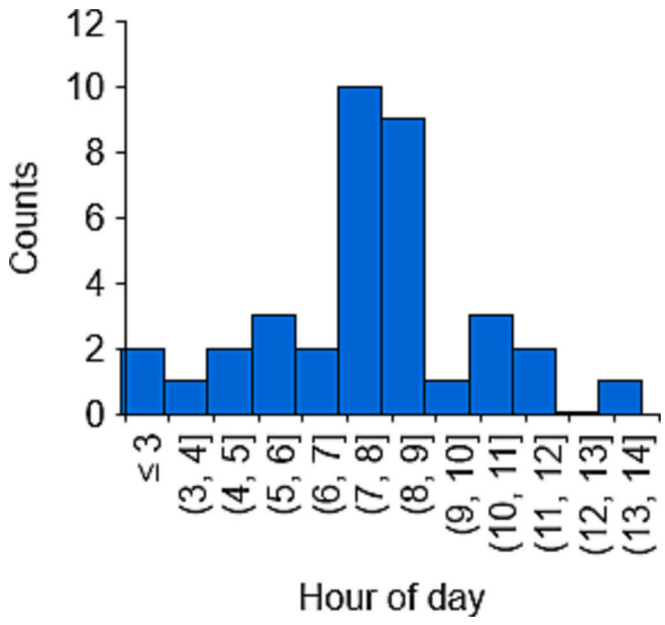

Fig. 11. Distribution of strip cycle initiation times for the 3 block system in the 7-week period where there is an overall surplus of PV.

an optimal pattern, where a block is stripped each day in a three-day cycle. This pattern is maintained until the system enters a prolonged PV deficit from week 7 onward, where the timing of the strip cycle has no effect on the SSR. The distribution of strip cycle initiation times in the stable period is shown in Fig. 11.

Fig. 11 shows that the optimal time for a strip cycle is in the AM hours, which are preferable to the PM hours as the RFB blocks hold a lower SOC on average, hence less energy must be discharged. The hours from 7 to 9 AM are selected most commonly, as this is the period in which site load and PV are most likely to be balanced. Hence these are the hours in which there is least requirement for the RFB to operate.

In the simulation performed without the strip cycle constraint, the 6 block system achieved higher SSR than the 3 block system, due to improvement energy efficiency achieved by tracking the optimum current more closely. When the strip cycle constraint is enforced, there is very little difference between the SSR profiles for the two systems as shown in Fig. 8.

In an islanded grid scenario, there would be an additional constraint on maintenance, where the RFB would be unable to drain quickly if load were not available. This would place additional importance on modularity, as the ability of empty modules to act as a sink for power would be even more useful.

4. Discussion

Although the range in power demand placed on the RFB system may be particularly extreme in this case study, significant variation is a universal feature of microgrids, and the modularity benefits demonstrated here should apply widely. The findings made for the Zn/Br RFB are in principle applicable to any hybrid flow battery, for example the soluble lead system [30].

One of the assumptions made in this work was that the site load and PV output are forecastable with 100 % accuracy over 24 h. The results are hence indicative of the best possible performance, which is still a valid basis for comparison. In practice, optimising the ensemble operation of the modules would require the definition of a set of rules for the control system. For example, if one module is online while the PV output is increasing, then a threshold power could be set where bringing the second module online would improve the ensemble efficiency. It was shown in Fig. 3 that when the single hybrid RFB is unable to meet all demands, it prioritises serving higher load as this can be done with lower losses. However, short-termist 'greedy' methods would not be able to make this judgement. Some form of learning method will likely be required to set appropriate thresholds for operation. Developing and demonstrating such a control system is a goal for the Active Classroom project. The work will also be expanded to include the energy transfer option, as the modules installed in the Active Classroom have the hardware necessary [28]. The use of 15-min resolution data in this work may lead to some inaccuracy, as it has been shown that meaningful differences in self-sufficiency measurement occur when moving from minute to second timescale [31].

Although system downtime due to strip cycles is reduced by modularity, there is a consequent power de-rating when this is occurring. This would not matter if there were consistent periods of low load in which taking one module out of action would have no impact. An encouraging finding from the current work is that the optimal time to do maintenance is when the PV output and load are closely matched, in which case the de-rating does not matter. A fuller analysis of the optimal sizing of the RFB and PV combined with a techno-economic analysis would be a useful study for the future. It is also important to remember that the maintenance requirement in the simulation is stricter than in reality, being based on 72 h of clock time rather than active time.

In the model, one simplification of reality was the neglect of energy consumption to run the pump for two hours during a strip cycle (120 Wh per module). In the first 30 days of operation, the six-module ensemble required 60 strip cycles ($6 \times 30 \times 24/72$), using 7.2 kWh. In this period, the modelled energy input to the modules was 791 kWh and the output was 575 kWh, giving an efficiency of 72.7 %. In practice, the output would decrease to 568 kWh, giving a very small decrease in efficiency to 71.8 %.

The results reported above show the benefit of modularity with appropriate control for a hybrid RFB, in terms of avoiding downtime and improving energy efficiency in order to maximise SSR. In this work, although SSR has been used as the objective, the site is modelled as being grid-tied, hence power can be exported. Some systems will by necessity be true micro-grids, in which case the SSR findings are directly relevant, but in the UK and other industrialised nations the majority of buildings are grid-tied. One of the focuses of running a battery within the Active Classroom is to demonstrate an additional building can be added to the grid without contributing either to overall energy demand or peak load of the grid. However, the use of SSR as an objective has been criticised as this metric does not always correlate with system wide benefit, and aiming for 100 % SSR can necessitate inefficient oversizing of the battery [24], or increased CO_2 emissions at the national level [32]. Also, at present in the UK, despite good progress on renewable power rollout, there have been no periods of national surplus so far, hence the marginal generation is usually open cycle gas turbines (OCGT), although the evening peak in wholesale price implies some plant have higher running costs than others, which may be due to poorer efficiency. If these differences are modest, then round trip losses may result in higher emissions when a battery is deployed. Using CO_2 minimisation as an objective may be more appropriate. Although real time grid CO_2 intensity data are not currently published, it would be a trivial matter to adjust the economic objective applied here to a CO_2 minimisation one.

5. Conclusions

In this work, a model was developed for deterministic optimisation of multiple hybrid RFB modules in order to maximise operational efficiency and avoid downtime due to maintenance. When the RFB is required to maximise self-sufficiency from PV at a site with highly varying load, it was predicted that using six independently controlled modules doubles the operational efficiency from 36 % to 73 %. This could be achieved primarily by idling modules when the power requirement is low in order to minimise parasitic losses. Additionally, the modular system is able to maintain an average SOC above zero,

despite the periodic maintenance downtime requirements, hence maintaining 100 % SSR where weekly PV availability permits. The novel modelling approach developed here allows the discovery of a non-obvious modular strategy whereby energy may be transferred from a module that is due a maintenance cycle to one which is freshly stripped, rather than discarding it. By running the simulation over multiple days it was found that the optimal timing for maintenance is most commonly in the morning when the modules have lower SOC, and PV output and site load are roughly balanced.

The findings of this work are important, as they show that perceived shortcomings of hybrid RFB systems may be overcome by modular control strategies in a typical use case. Further work is required to translate the deterministic optimisation approach here to a rules-based approach that could be used for real-time control.

CRediT authorship contribution statement

Diarmid Roberts: Conceptualization, Formal analysis, Methodology, Visualization, Writing – original draft, Writing – review & editing. **Jenny Baker:** Conceptualization, Funding acquisition, Writing – original draft, Writing – review & editing. **Justin Searle:** Conceptualization, Funding acquisition, Writing – review & editing. **Tom Griffiths:** Conceptualization, Data curation, Investigation, Writing – review & editing. **Richard Lewis:** Investigation, Writing – review & editing. **Solomon Brown:** Conceptualization, Formal analysis, Funding acquisition, Methodology, Writing – original draft, Writing – review & editing.

Declaration of competing interest

The authors declare the following financial interests/personal relationships which may be considered as potential competing interests: Diarmid Roberts reports financial support was provided by Drax Power Ltd.

Data availability

The data-set used in this work, and the code used for the simulations may be found in the GitHub repository [25].

Acknowledgements

This work was supported by the Engineering and Physical Sciences Research Council (EPSRC) through SPECIFIC Innovation and Knowledge Centre (EP/N020863/1), and the CDT for Energy Storage and its Applications (EP/L016818/1). Dr. Jenny Baker was also funded through ECR Fellowship NoRESt (EP/S03711X/1). The work at Sheffield was also supported by Drax Group. The funding sources were not involved in decisions relating to the execution and publication of this work.

References

[1] L. Waters, “Energy Consumption in the UK (ECUK) 1970 to 2019,” 2020. [Online]. Available: https://assets.publishing.service.gov.uk/government/uploads/system/uploads/attachment_data/file/928350/2020_Energy_Consumption_in_the_UK_ECUK_.pdf.

[2] R. Hoggett, J. Ward, and C. Mitchell, “Heat in Homes: customer choice on fuel and technologies,” 2011. [Online]. Available: https://geography.exeter.ac.uk/staff_profile_images/Hoggett2011_Heat_in_Homes.pdf.

[3] J. Clarke, P. Jones, J. Littlewood, D. Worsley, Active buildings in practice, Sustain. Energy Build. Smart Innov. Syst. Technol. 163 (2020), https://doi.org/10.1007/978-981-32-9868-2_47.

[4] A. Mellor, et al., Roadmap for the next-generation of hybrid photovoltaic-thermal solar energy collectors, Sol. Energy 174 (Nov. 2018) 386–398, https://doi.org/10.1016/j.solener.2018.09.004.

[5] C. Brown, E. Perisoglou, R. Hall, V. Stevenson, Transpired solar collector installations in Wales and England, Energy Procedia 48 (Jan. 2014) 18–27, https://doi.org/10.1016/j.egypro.2014.02.004.

[6] J. Searle, S. Bishop, Energy exemplars, Prop. J. Jan-Feb (2020) 36.

[7] “Specific Project Active Office And Classroom.” https://my.matterport.com/show/?m=AYAXCEfU7zM (accessed May 25, 2021).

[8] Y. K. Zeng, T. S. Zhao, L. An, X. L. Zhou, and L. Wei, “Zeng (2015) A comparative study of all-vanadium and iron-chromium redox flow batteries for large-scale energy storage.pdf,” *Journal of Power Sources*, vol. 300. Elsevier, pp. 438–443, Dec. 30, 2015, doi: https://doi.org/10.1016/J.JPOWSOUR.2015.09.100.

[9] L. Su, A. F. Badel, C. Cao, J. J. Hinricher, and F. R. Brushett, “Toward an inexpensive aqueous polysulfide–polyiodide redox flow battery,” Ind. Eng. Chem. Res., vol. 56, no. 35, pp. 9783–9792, Sep. 2017, doi:https://doi.org/10.1021/acs.iecr.7b01476.

[10] S. Rathod, N. Jaiswal, M.K. Ravikumar, S. Patil, A. Shukla, Effect of binary additives on performance of the undivided soluble-lead-redox-flow battery, Electrochim. Acta 365 (Jan. 2021) 137361, https://doi.org/10.1016/j.electacta.2020.137361.

[11] M.C. Wu, T.S. Zhao, H.R. Jiang, Y.K. Zeng, Y.X. Ren, High-performance zinc bromine flow battery via improved design of electrolyte and electrode, J. Power Sources 355 (Jul. 2017) 62–68, https://doi.org/10.1016/j.jpowsour.2017.04.058.

[12] A. Parasuraman, T. M. Lim, C. Menictas, and M. Skyllas-Kazacos, “Review of material research and development for vanadium redox flow battery applications,” *Electrochimica Acta*, vol. 101. Pergamon, pp. 27–40, Jul. 01, 2013, doi:https://doi.org/10.1016/j.electacta.2012.09.067.

[13] K. Orapeleng, R.G.A. Wills, A. Cruden, Developing electrolyte for a soluble lead redox flow battery by reprocessing spent lead acid battery electrodes, Batteries 3 (2) (2017) 1–13, https://doi.org/10.3390/batteries3020015.

[14] M. K. Ravikumar, S. Rathod, N. Jaiswal, S. Patil, and A. Shukla, “The renaissance in redox flow batteries,” Journal of Solid State Electrochemistry, vol. 21, no. 9. Springer New York LLC, pp. 2467–2488, Sep. 01, 2017, doi:https://doi.org/10.1007/s10008-016-3472-4.

[15] Redflow, “ZBM2 Flow Battery,” 2019. Accessed: May 20, 2021. [Online]. Available: https://redflow.com/wp-content/uploads/2019/10/Redflow-ZBM2-datasheet-1910-Public-Web.pdf.

[16] M. Raugei, M. Kamran, A. Hutchinson, A prospective net energy and environmental life-cycle assessment of the UK electricity grid, Energies 13 (9) (May 2020) 2207, https://doi.org/10.3390/en13092207.

[17] Networks, “UK's largest flow battery system connected to grid,” 2017. https://networks.online/power/uks-largest-flow-battery-system-connected-to-grid/ (accessed May 20, 2021).

[18] Energy Storage Journal, “UK ESS PROJECT TO BE WORLD'S BIGGEST LI-ION-VRFB HYBRID,” 2019. https://www.energystoragejournal.com/uk-ess-project-to-be-worlds-biggest-li-ion-vrfb-hybrid/ (accessed Dec. 03, 2021).

[19] Z. Xu, Q. Fan, Y. Li, J. Wang, and P. D. Lund, “Review of zinc dendrite formation in zinc bromine redox flow battery,” *Renewable and Sustainable Energy Reviews*, vol. 127. Elsevier Ltd, p. 109838, Jul. 01, 2020, doi:https://doi.org/10.1016/j.rser.2020.109838.

[20] D. Roberts, S. Brown, Flow batteries for energy management: novel algebraic modelling approaches to properly assess their value, J. Energy Storage 26 (2019), https://doi.org/10.1016/j.est.2019.100977.

[21] International Flow Battery Forum, Panel Discussion: ‘Why Choose a Flow Battery?’, 2021.

[22] W.E. Hart, et al., Pyomo — Optimization Modeling in Python 67, 2017.

[23] H.P. Williams, Model Building in Mathematical Programming, Wiley (2013) 142.

[24] S.I. Sun, M. Kiaee, S. Norman, R.G.A. Wills, Self-sufficiency ratio: an insufficient metric for domestic PV-battery systems? Energy Procedia 151 (Oct. 2018) 150–157, https://doi.org/10.1016/j.egypro.2018.09.040.

[25] D. Roberts, MEEM (source code). https://github.com/diarmidr/MEEM, 2021.

[26] H.E. William, J.-P. Watson, D.L. Woodruff, Pyomo: modeling and solving mathematical programs in Python, Math. Program. Comput. 3 (3) (2011) 219.

[27] Gurobi Optimization inc., “Mathematical Programming Solver | Gurobi.” http://www.gurobi.com/products/gurobi-optimizer.

[28] Redflow, Installation and Operation Manual ZBM2 (3kW/10kWh) v4.0 [Online]. Available: https://redflow.com/wp-content/uploads/2018/03/ZBM2-Installation-and-Operation-Manual-CE-V2.9.pdf, 2019.

[29] Sandia National Laboratories, “Initial test results from the RedFlow 5 kW, 10 kWh zinc-bromide module, phase 1.” [Online]. Available: https://www.osti.gov/biblio/1039005.

[30] M. Krishna, E.J. Fraser, R.G.A. Wills, F.C. Walsh, Developments in soluble lead flow batteries and remaining challenges: an illustrated review, J. Energy Storage 15 (2018) 69–90, https://doi.org/10.1016/j.est.2017.10.020.

[31] A. Ayala-Gilardón, M. Sidrach-de-Cardona, L. Mora-López, Influence of time resolution in the estimation of self-consumption and self-sufficiency of photovoltaic facilities, Appl. Energy 229 (Nov. 2018) 990–997, https://doi.org/10.1016/j.apenergy.2018.08.072.

[32] M. Beuse, B. Steffen, M. Dirksmeier, T.S. Schmidt, Comparing CO2 emissions impacts of electricity storage across applications and energy systems, Joule 5 (2021) 1501–1520, https://doi.org/10.1016/j.joule.2021.04.010.